


**Influence of phonon harmonicity on spectrally pure resonant Stokes fields**Georgios Stoikos<sup>\*</sup> and Eduardo Granados<sup>†</sup>  
CERN, 1217 Geneva, Switzerland (Received 16 March 2022; accepted 21 July 2022; published 3 August 2022)

Due to their highly coherent emission, tunability, and compactness, integrated single-frequency diamond Raman lasers are interesting tools for applications in integrated quantum technology, high-resolution spectroscopy, or coherent optical communications. While the fundamental emission linewidth of these lasers can be Fourier limited, their thermo-optic characteristics lead to drifts in their carrier frequency, posing important challenges for applications requiring ultrastable emission. We propose here a method for measuring accurately the temperature-dependent index of refraction of diamond by employing standing Stokes waves produced in a monolithic Fabry-Pérot diamond Raman resonator. Our approach takes into account the influence of temperature on the first-order phonon line and the average lattice phonon frequency under intense stimulated Raman scattering conditions. We further utilize this model to calculate the value of the average phonon frequency and then the temperature-dependent thermo-optic coefficient. The theory is accompanied by the demonstration of tunable Fourier-limited Stokes nanosecond pulses with a stabilized center frequency deviation of less than 4 MHz.

DOI: [10.1103/PhysRevA.106.023504](https://doi.org/10.1103/PhysRevA.106.023504)**I. INTRODUCTION**

Spectrally pure, tunable, and ultrastable light sources have become one of the main tools for advancing scientific and technological quantum applications. These include the development of atomic clocks, LIDAR, or quantum ion computers to name a few [1,2]. The interest in building and integrating such light sources indicates the need for scalable architectures to cool, trap, and manipulate multiple ions simultaneously [3]. The main challenge here is in the complexity of producing widely tunable, high-performance narrow-band lasers (in tens of MHz and below) at a range of wavelengths from the UV to the near-IR.

In this regard, the field of diamond Raman lasers has experienced a renaissance since they can provide directly single-frequency light at nearly any optical wavelength [4–7]. Stimulated Raman scattering (SRS) has specific advantages that make it interesting for this task. For instance, the non-linear process is mediated by propagating pump photons rather than via energy storage in localized ions, so there is no spatial hole burning or axial mode competition [7]. The phase-matching condition between pump and Stokes beams is automatically satisfied, and therefore the energy transfer relationship between waves depends on the shape and overlap of their temporal envelopes instead of their spectral distribution or phase characteristics. In certain cases, the Stokes

spectrum can be driven to duplicate that of the pump spectrum in the so-called high-gain regime [8,9], which underpins the production of single-frequency nanosecond pulses when using spectrally broad pump lasers [10].

In addition, optical devices such as cavities, resonators, and optomechanical components realized in single-crystal diamond are poised to benefit from its extraordinary material properties. The interest in diamond is further propelled by its wide use for quantum applications [11], including quantum computing, generation of single photons [12], quantum sensing [13], and quantum memories [14]. Moreover, the production of tunable narrow-linewidth output from a Fabry-Pérot (FP) integrated diamond resonator was recently demonstrated, without the need of external mechanical feedback loops to control the cavity length [15].

Within this framework, knowledge of the thermo-optic coefficient is of paramount importance for integrated photonic devices based on diamond, and the present research was conducted with the purpose of gaining insight into accurate prediction of tuning the Stokes resonant frequency in integrated diamond resonators. Unfortunately, the existing approximations for the index of refraction render them insufficient for the level of accuracy required in the aforementioned applications.

When it comes to the refractive index of diamond, there have been many works relative to the optical and Raman properties of diamond, but there is a scarcity of information regarding the index of refraction under strong vibrational fields and at different temperatures. The work of Ruf *et al.* [16] provided valuable information for estimating the thermo-optic coefficient; however, it did not take into account the overall contribution of the different temperature-dependent vibrational modes that can be produced in diamond, and thus it needs to be expanded upon.

<sup>\*</sup>Also at School of Applied Mathematics and Physical Sciences, National Technical University of Athens.

<sup>†</sup>eduardo.granados@cern.ch

Published by the American Physical Society under the terms of the [Creative Commons Attribution 4.0 International license](https://creativecommons.org/licenses/by/4.0/). Further distribution of this work must maintain attribution to the author(s) and the published article's title, journal citation, and DOI.

We propose here an alternative methodology for measuring and calculating the thermo-optic coefficient. Our methodology includes the use of a monolithic single-frequency FP diamond Raman resonator operating at visible wavelengths. Here the accurate measurement of the output Stokes frequency as a function of temperature allows us to retrieve the temperature-dependent index of refraction that produced a frequency shift in the Stokes field output. For this method to be efficient, the use of diamond Raman monolithic resonators is important because they provide an ultrastable environment that depends exclusively on the resonator thermo-optic properties and not the pumping laser characteristics or the environment.

Additionally, we demonstrate that the production of tunable Fourier-limited Stokes few nanosecond pulses with a stabilized center frequency deviation of less than  $< 4$  MHz is readily available, where the temperature stability of the bulk crystal is a key parameter for enhanced performance. Our theoretical model suggests that cooling the diamond resonator below 200 K may have additional advantages due to the reduced thermo-optic coefficient in that temperature range, enhanced gain, and reduced Raman linewidth.

## II. MEASUREMENT PRINCIPLE

In terms of using the diamond bulk as a Raman laser material, its unique optical properties has enabled the development of lasers operating over a wide spectrum due to its giant Raman frequency shift ( $1332 \text{ cm}^{-1}$ ), large Raman gain ( $> 40 \text{ cm/GW}$  at 532 nm), and ultrawide transparency window (from deep ultraviolet all the way to THz, except for a lossy window from  $2.6\text{--}6 \mu\text{m}$  due to multiphonon-induced absorption [8,17–21]). Furthermore, the excellent thermal properties afforded by diamond (unsurpassed thermal conductivity of  $1800 \text{ W/m/K}$  at 300 K and low thermo-optic coefficient of the order of  $10^{-5} \text{ K}^{-1}$ ) along with negligible birefringence [22] make it an ideal material for high-power Raman lasing with greatly reduced thermal lensing effects at the kW average power level [23].

The generation of single longitudinal mode (SLM) or narrow linewidth light via SRS in diamond remained elusive until relatively recently [5,7,24–26]. Such bulk cavity systems also require precise alignment, elaborated feedback loops, and maintenance of optical components for the laser to function robustly. The further integration of SLM Raman lasers in diamond was recently demonstrated [10], showing that by embedding the laser resonator in the Raman media, it was possible to produce frequency stable output from a FP diamond resonator without the need of external mechanical feedback loops to control the cavity length. Moreover, these resonators performed complex functions such as “linewidth squeezing” when pumped by few GHz linewidth multimode lasers. Such mechanism, supported by phonon-resonant Raman interactions, directly enhanced the available power spectral density of broadband nanosecond lasers by nearly two orders of magnitude.

The frequency stabilization of these FP diamond resonators was carried out by adjusting the temperature of the diamond substrate, which simultaneously influenced the index of refraction, size, and Raman shift of the Raman resonator [15].

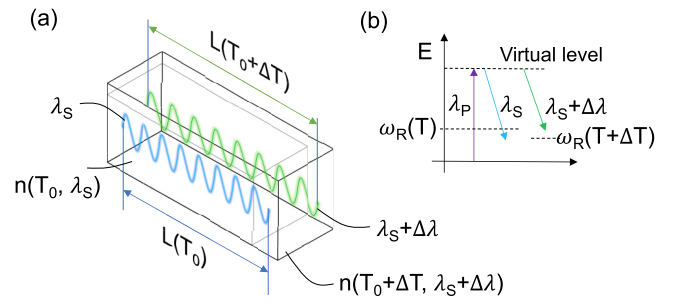


FIG. 1. (a) Schematic depiction of main thermal effects influencing the resonant Stokes frequency in a monolithic Raman resonator, and (b) depiction of the temperature effect on the photon and optical phonon energies.

In this work we shine light into that complex interplay of thermo-optical and Raman effects by studying their dependency on temperature, allowing us to construct a theoretical model capable of predicting with accuracy the resonating Stokes frequency. Our model is accompanied by an experimental demonstration showing excellent agreement with the proposed theory.

We start by identifying the main factors affecting the resonant Stokes frequency as well as their temperature dependency. Those are depicted in Fig. 1, where we have separated the temperature effects on the material optical properties and size [Fig. 1(a)] and the effects on the Raman shift center frequency  $\omega_R$  [Fig. 1(b)]. In terms of the Stokes resonating frequency, the index of refraction depends simultaneously on the temperature and the chromatic dispersion [ $n(T, \lambda)$ ] due to the shifted Stokes wavelength  $\lambda'_S = \lambda_S + \Delta\lambda(T)$ . Note that all wavelengths used in this work are in vacuum. The thermal expansion process simultaneously affects the resonating wavelength due to the variable boundary condition [the diamond length  $L(T)$  shifts to  $L(T + \Delta T)$ ]. Likewise, the Raman shift center frequency  $\omega_R(T)$  tuning with temperature does not establish the resonating wavelength or the tuning slope as a function of temperature, but it does affect the location of the boundaries of the longitudinal mode hopping in frequency. We describe all these effects in detail in the following sections, followed by the experimental results.

## III. SINGLE-FREQUENCY OPERATION OF MONOLITHIC FABRY-PÉROT DIAMOND RAMAN RESONATORS

The production of single-frequency resonant Stokes fields depends on many factors, but most importantly on the characteristics of the pump laser intensity, wavelength, and linewidth, resonator optical length, and temporal envelope of the interplaying pump and Stokes pulses.

The temporal features of these laser fields, in both amplitude and phase on timescales shorter than the resonator round-trip time, are caused by the interference of its spectral longitudinal modes. These modes, however, generally vary in amplitude and phase on the timescale of the round-trip time or slower. Since the longitudinal modes vary slowly (much slower than the phonon dephasing time, in diamond  $T_2 \approx 6.8$  ps), we can use steady-state Raman theory, even if interference of the modes produces structures that would

need transient Raman theory if modeled in the time domain. This approach has been widely used to analyze SRS with broad-band lasers [27–33], and here we employ this method to model the diamond Raman resonator since it is computationally efficient for nanosecond pulses with GHz-class linewidths.

To construct the frequency domain model we follow the same strategy as in [10,27], but ultimately adapted to single-frequency pump fields. Nevertheless, the mathematical treatment is analogous, and here we include it for completeness. We start by writing the general equations for a fundamental field (or “pump”) with  $2m + 1$  modes spaced in frequency by  $\Omega_F$ , and a multimode Stokes field with  $2m + 1$  modes spaced in frequency by  $\Omega_F$ :

$$\tilde{E}_F = \sum_{l=-m}^m F_l e^{i(\omega_{F(l)}t - k_{F(l)}z)} + \text{c.c.}, \quad (1)$$

$$\tilde{E}_S = \sum_{l=-m}^m S_l e^{i(\omega_{S(l)}t - k_{S(l)}z)} + \text{c.c.}, \quad (2)$$

in which c.c. represents the complex conjugate of the preceding term,  $\omega_{S(l)} = \omega_{S(0)} + \Omega_F l$ , and  $\omega_{F(l)} = \omega_{F(0)} + \Omega_F l$ . In these equations,  $S_l$  and  $F_l$  are complex amplitudes describing the amplitude and phase of the modes traveling inside the diamond. The approximations for the mode wave vector  $k_{F(l)} \approx k_{F(0)} + \Omega_F l / u_F$  accounts for the group velocity difference between the fundamental wave packets, but neglect group velocity dispersion within each wave packet. Analogously for the Stokes field the mode wave vector  $k_{S(l)} \approx k_{S(0)} + \Omega_F l / u_S$ .

In the following we assume that the central Stokes mode  $S_0$  is centered within the Raman gain linewidth so that it accesses the highest or monochromatic Raman gain. Note that in our model the following identity is always true:

$$\omega_{F(l)} = \omega_{S(l)} + \omega_R; \quad (3)$$

here  $\omega_R$  is the frequency of the Raman shift at the line center. This essentially is to say that the modes of fundamental and Stokes fields are paired. In order to describe the coupling between this set of modes, we rely on steady-state Raman formalism and write it in a nondegenerate mode for four generic modes  $F_{l_1}$ ,  $F_{l_2}$ ,  $S_{l_3}$ , and  $S_{l_4}$ :

$$\frac{1}{u_S} \frac{\partial S_{l_4}}{\partial t} \pm \frac{\partial S_{l_4}}{\partial z} \propto F_{l_1} (F_{l_2}^* S_{l_3}). \quad (4)$$

This was interpreted in [27] as two modes ( $F_{l_2}^* S_{l_3}$ ) driving a phonon field and a third mode  $F_{l_1}$  scattering off the phonon field to drive a fourth mode  $S_{l_4}$ . For fundamental and Stokes pulsed fields with many longitudinal modes or broadband modes, in principle all types of interactions can drive a polarization at the frequency of a generic mode  $S_{r_2}$ , given that they satisfy the equation

$$\omega_{S_{r_2}} = \omega_{F_{l_1}} - \omega_{F_{l_2}} + \omega_{S_{l_3}}. \quad (5)$$

Now Eq. (4) can be used as template to reformulate the amplification of a generic Stokes mode  $S_l$  and the depletion

of the fundamental modes  $F_l$  as a function of the other three interacting waves as follows:

$$\frac{1}{u_S} \frac{\partial S_l}{\partial t} + \frac{\partial S_l}{\partial z} = 2cn_F \epsilon_0 \frac{g_0}{2} \sum_r \sum_j F_{l-r} (S_j F_{j-r}^*) \times \frac{\Delta\omega_R}{\Delta\omega_R - ir\Omega_F} e^{i(l-j)\mu_{\pm}\Omega_F z}, \quad (6)$$

$$\frac{1}{u_F} \frac{\partial F_l}{\partial t} + \frac{\partial F_l}{\partial z} = -2cn_S \epsilon_0 \frac{g_0}{2\eta} \sum_r \sum_j S_{l-r} (F_j S_{j-r}^*) \times \frac{\Delta\omega_R}{\Delta\omega_R + ir\Omega_F} e^{i(j-l)\mu_{\pm}\Omega_F z}. \quad (7)$$

The parameter  $\mu_{\pm}$  is the group delay difference per meter between the fundamental and Stokes waves. The positive part  $\mu_+$  accounts for copropagating waves or forward SRS and the negative  $\mu_-$  for the backward SRS:

$$\mu_{\pm} = \frac{1}{u_F} \mp \frac{1}{u_S}. \quad (8)$$

Equations (6) and (7) account for all the combinations between pump and Stokes modes. The resulting spectra for the Stokes field are dependent on the relative amplitudes of the resonant and nonresonant terms. The resonant terms ( $r = 0$ ) have the phonon driving term exactly resonant with the phonon frequency and can access the highest gain, while other nonresonant interactions have a detuning  $r\Omega_F$  that reduces gain and causes a phase rotation. For our model, both resonant and nonresonant interactions need to be taken into account since  $\Delta\omega_R > \Omega_F$ .

Degenerate terms ( $j = l$ ) have no phase mismatch terms ( $\Delta k = 0$ ) even in the presence of dispersion, and because of the degeneracy these terms must always have the correct phase to provide gain. Nondegenerate modes, however, can be neglected in dispersive media where the phase mismatch is  $\Delta k \approx (l - j)\Omega_F \mu_{\pm}$ , and so these terms will oscillate in and out of phase with the waves they drive. Here we assume that dispersion in diamond is large enough in the UV and visible spectral ranges to neglect nondegenerate mixing modes without loss of accuracy. With this approximation, we can rewrite Eqs. (6) and (7) forcing  $j = l$ . Likewise, for the specific case of single longitudinal mode pumping, the equations can be further simplified to

$$\frac{1}{u_S} \frac{\partial S_l}{\partial t} + \frac{\partial S_l}{\partial z} = 2cn_F \epsilon_0 \frac{g_0}{2} F_0 (S_l F_0^*) \frac{\Delta\omega_R}{\Delta\omega_R + il\Omega_F}, \quad (9)$$

$$\frac{1}{u_F} \frac{\partial F_0}{\partial t} + \frac{\partial F_0}{\partial z} = -2cn_S \epsilon_0 \frac{g_0}{2\eta} \sum_r S_r (F_0 S_r^*) \frac{\Delta\omega_R}{\Delta\omega_R + ir\Omega_F}. \quad (10)$$

The term  $\Delta\omega_R / (\Delta\omega_R - ir\Omega_F)$  reduces the gain of off-resonant terms by a Lorentzian factor  $1 + (r\Omega_F / \Delta\omega_R)^2$ , and therefore the most efficient interaction is always for doubly degenerate resonant interactions.

Let's assume now that the combination of pump intensity and resonator losses is adequate so that the amplification is highly preferential for the central mode  $S_0$  as in [10] and is capable of depleting the fundamental field. This configuration will produce the minimal linewidth for a given resonator round-trip loss and can also occur when the FSR of the

diamond resonator is larger than the effective Raman gain linewidth. A way of calculating the resulting Stokes linewidth is by further simplifying Eqs. (9) and (10) by implying  $\{S_l = 0 \forall l \neq 0\}$ :

$$\frac{1}{u_S} \frac{\partial S_0}{\partial t} + \frac{\partial S_0}{\partial z} = 2cn_F \epsilon_0 \frac{g_0}{2} |F_0|^2 S_0, \quad (11)$$

$$\frac{1}{u_F} \frac{\partial F_0}{\partial t} + \frac{\partial F_0}{\partial z} = -2cn_S \epsilon_0 \frac{g_0}{2\eta} |S_0|^2 F_0. \quad (12)$$

We can now use Eqs. (11) and (12) to model the dynamic interplay between fundamental and Stokes waves in the Raman resonator when the fields are located at the Raman gain line center. Intuitively, it is possible to see in Eq. (11) that the temporal envelope of the Stokes field depends only on the amplitude of the fundamental pumping pulse and not its phase, whereas the resonating Stokes wavelength will depend only on the resonator geometry and optical characteristics and not the pump field. The resulting Stokes linewidth, however, will be directly linked to the pump pulse temporal envelope and dispersion characteristics of the resonator, the generation of nearly Fourier-limited pulses when low-noise pump pulses are used is relatively straightforward.

For the case of a temperature tuned Stokes frequency, the mismatch between the Raman gain line center and the resonating Stokes field will produce a reduced gain by a factor  $1 + (\Delta\omega_S(T)/\Delta\omega_R)^2$  due to the detuned Stokes mode. Here  $\Delta\omega_S(T)$  is the frequency shift produced in the resonator due to temperature. The calculation of this shift is described in the next section.

#### IV. RELATIONSHIP BETWEEN THE STOKES CENTER FREQUENCY AND THE REFRACTIVE INDEX

Knowledge of diamond's optical and mechanical properties runs deep for most factors, with an exception being the temperature dependence of the refractive index (also known as thermo-optic coefficient), despite its importance for optical applications or integrated photonic devices in diamond. In the literature it is usually found as a single value of  $(1/n)\partial n/\partial T = 5 \times 10^{-6} \text{ K}^{-1}$  at 300 K for the low-frequency limit [34] or in the far-infrared range for a temperature range of up to 925 K [16]. Precise information regarding the thermo-optic coefficient of diamond at visible wavelengths and at extended temperature ranges remains relatively unknown.

A thorough theoretical description on the thermo-optic coefficient in diamond is a great challenge since it requires a working model for the dielectric function and its renormalization by the electron-phonon interaction and the thermal expansion of the lattice [16]. There have been models using empirical pseudopotentials for the thermo-optic coefficients of different semiconductors, but since C has a large Debye temperature  $\Theta_D = 1880 \text{ K}$ , knowledge of the thermo-optic coefficient at 300 K does not provide meaningful information for higher temperatures [35]. The inaccuracy is caused by the fact that a linear approximation of the temperature-dependent index of refraction  $n(T)$  is permitted at temperatures much larger than  $\Theta_D$  where the material can be described by a single oscillator frequency.

In the following we present a methodology for the calculation of the Stokes frequency and its tuning slope for a generic monolithic Raman resonator longitudinal mode and its relation to the temperature-dependent refractive index. We start with the condition for resonance within the diamond FP resonator:

$$\nu_S(T_0) = q \frac{c}{2L_{\text{eff}}(T_0, \nu_S)}, \quad (13)$$

where  $q$  is the mode number,  $c$  is the speed of light in vacuum, and  $L_{\text{eff}}(T_0, \nu_S)$  is the effective length of the resonator at the Stokes resonating frequency  $\nu_S$  and at temperature  $T_0$ .  $L_{\text{eff}}$  can be calculated as  $L_{\text{eff}}(T_0, \nu_S) = L(T_0)n(\lambda_S, T_0)$ , where  $n(\lambda_S, T_0)$  is the wavelength-temperature dependent index of refraction, and  $L(T_0)$  is the resonator physical length at temperature  $T_0$ . In [16] the temperature-dependent part of the refractive index  $n_T(T)$  was separated from the wavelength-dependent part  $n_\lambda(\lambda)$ . The two terms are added together to give the total index of refraction as

$$n(\lambda, T) = n_\lambda^0(\lambda) + n_T(T). \quad (14)$$

We note that  $n_\lambda^0(\lambda)$  refers to the Sellmeier equation at 0 K, and  $n_T(T)$  represents the change of index due to temperature at a fixed wavelength. For small shifts in temperature ( $\Delta T$ ) we can use a perturbation theory approach to estimate the resulting wavelength shift of the Stokes by

$$\begin{aligned} \lambda_S(T_0 + \Delta T) &= \frac{2}{q} \left( L(T_0) + \frac{\partial L}{\partial T} \Delta T \right) \\ &\times \left( n(T_0, \lambda_S) + \frac{\partial n}{\partial T} \Delta T + \frac{\partial n}{\partial \lambda} \Delta \lambda_S \right). \end{aligned} \quad (15)$$

Here the term  $\partial L/\partial T$  can be expressed in terms of the linear thermal expansion coefficient ( $\alpha$  in the following) as  $\partial L/\partial T = \alpha L(T_0)$ . The shift in wavelength can be directly calculated by  $\Delta \lambda_S = \lambda_S(T_0 + \Delta T) - \lambda_S(T_0)$ . The terms  $\partial n/\partial T$  and  $\partial n/\partial \lambda$  correspond to the thermo-optic coefficient at  $T_0$  and the chromatic dispersion at  $\lambda_S$ , respectively. Here we assume that dispersion terms do not change for small temperature increments  $\Delta T$ .

Reorganizing Eq. (15) and neglecting second-order differential terms, we can obtain the tuning slope of the center Stokes wavelength as a function of temperature:

$$\left. \frac{\partial \nu_S}{\partial T} \right|_{T_0} = -c \frac{\frac{1}{n} \frac{\partial n_T}{\partial T} + \alpha(T)}{\lambda_S \left( 1 - \frac{\lambda_S}{n} \frac{\partial n_\lambda}{\partial \lambda} \right)}, \quad (16)$$

where  $c$  is the speed of light in vacuum,  $n$  the index of refraction of diamond at the Stokes wavelength and at temperature  $T_0$ , and  $\alpha(T)$  the temperature-dependent thermal expansion coefficient of CVD diamond. Jacobson *et al.* modeled  $\alpha(T)$  in [36] having the following form:

$$\alpha(T) = \sum_{i=1}^n X_i E \left( \frac{\Theta_i}{T} \right), \quad (17)$$

where  $E(x)$  corresponds to the function given by

$$E(x) = \frac{x^2 e^x}{(e^x - 1)^2}. \quad (18)$$

Experimental values for  $X_i$  and  $\Theta_i$  can be found in [36], and those are the ones used here for the calculations.

Continuing,  $\frac{1}{n} \frac{\partial n_T}{\partial T}$  is the thermo-optic coefficient. Typical values for this coefficient in the literature are approximately  $5 \times 10^{-6} \text{ K}^{-1}$  [34]. The key part here is in the understanding of the temperature-dependent term  $n_T(T)$ , which requires one to identify the effects that influence it. In general, the index of refraction depends on the lattice energy, which here it is assumed to be proportional to the internal energy of the system [37]. For diamond, it is possible to use a Bose-Einstein distribution to describe the unit cell infrared active vibration [38].

As a consequence, we can refer to the approximation of the temperature-dependent index of refraction as  $n_T(T)$  described in [16]:

$$n_T(T) = A \left( \frac{1}{e^{\frac{\hbar\omega_0}{k_B T}} - 1} + \frac{1}{2} \right) \quad (19)$$

with the first term being the Bose-Einstein distribution. Ruf *et al.* [16] estimated the values of  $A$  and  $\hbar\omega_0$  based on fits of the data to their experimental measurements. Their results retrieved a value of  $A = 0.01902$  and an average phonon frequency of  $\hbar\omega_0 = 711 \text{ cm}^{-1}$ , independent of temperature. Even though the results in that work fit well their experiments, the influence of the thermal expansion of the lattice to the vibrational eigenfrequencies and multiphonon coupling effects (see, for example, [39]) were not taken into account, nor their contribution to the line shift of the average phonon frequency  $\omega_0$ .

When it comes to the wavelength-dependent part of the index of refraction  $n_\lambda(\lambda)$ , we are basing our model in the most recent single-term Sellmeier equation found for synthetic diamond [40]. The Sellmeier equation is usually calculated at room temperature (300 K), but the separable equation for the index of refraction in Eq. (14) requires the index at absolute zero temperature. To that end, we approximated  $n_\lambda^0(\lambda)$  as follows:

$$n_\lambda^0(\lambda) = n_\lambda(\lambda) - n_T(300). \quad (20)$$

The factor  $n_T(300)$  was calculated using Eq. (14) at 300 K. In this way we also guarantee that the index of refraction is the one commonly known at room temperature.

In terms of the temperature dependence of the Raman shift, it defines the spectral range where the monolithic resonator will lase, although not the specific frequency of the Stokes standing waves. Having this in mind, we present here for completeness the dependency of the first-order phonon frequency (or Raman shift) on temperature. The Klemens anharmonic approximation assumes that the zone-center phonon decay into two acoustical phonons of opposite momentum is appropriate to describe the effects in the diamond lattice [41,42]. In that model the relaxation time  $\tau$  is

$$\tau \simeq 1 + \frac{2}{e^{\frac{\hbar}{k_B T} \frac{\omega_R}{2}} - 1}, \quad (21)$$

where  $\omega_R$  is the Raman shift. The relaxation time  $\tau$  is proportional to the Raman linewidth  $\Delta\omega_R$  and that later is linearly connected to the Raman shift [43]. The temperature-

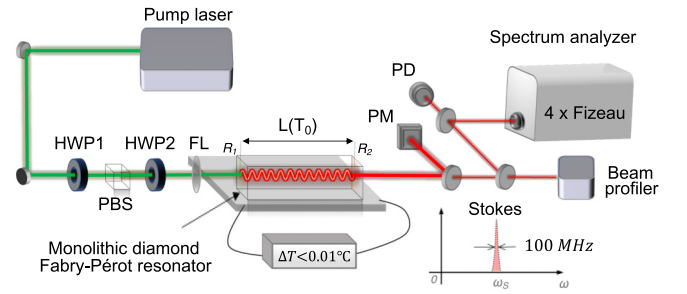


FIG. 2. Schematic layout of the experimental setup: A monolithic diamond resonator is pumped by a frequency-doubled Q-switched Nd:YAG laser. The output Stokes nanosecond pulse was characterized temporally and spectrally with a set of four high-resolution Fizeau interferometers, and a photodiode (PD) connected to a large bandwidth 16 GHz oscilloscope. HWP1, HWP2: half-wave plates; PBS: polarizing beam splitter; FL: focusing lens; PM: power meter.

dependent Raman shift is then given by

$$\omega_R(T) = 1332.7 - A_R \left( \frac{2}{e^{\frac{\hbar\omega_R}{2k_B T}} - 1} \right) \frac{10^7}{c} [\text{cm}^{-1}], \quad (22)$$

where  $A_R$  depends on the dispersion lines of diamond [43]. A fit to the experimental data shown in [44] resulted in  $A_R = 2.6 \times 10^3 \text{ GHz}$ . We are now ready to experimentally measure  $\partial\nu_S/\partial T$  and fit it to our model, allowing us to extract the thermo-optical coefficient of diamond.

## V. EXPERIMENT

In order to confirm our method, we have set up an experiment to analyze the Stokes resonant frequency in the resonator as a function of temperature with high accuracy. From these data we can then relate the constants and tuning slope-related physical parameters.

A temperature-adjustable monolithic FP diamond resonator was used in our experiments as the tool for measuring

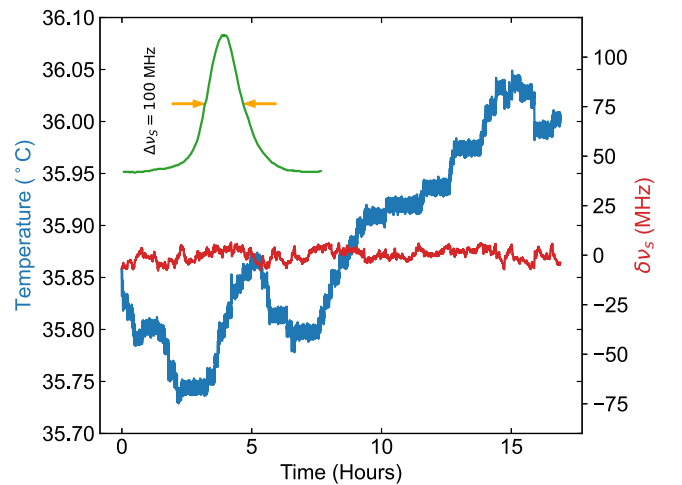


FIG. 3. Active temperature stabilization of the Stokes resonant frequency over more than 16 h. The RMS fluctuation of the Stokes frequency is less than 4 MHz. Inset: Measured Stokes field spectrum.

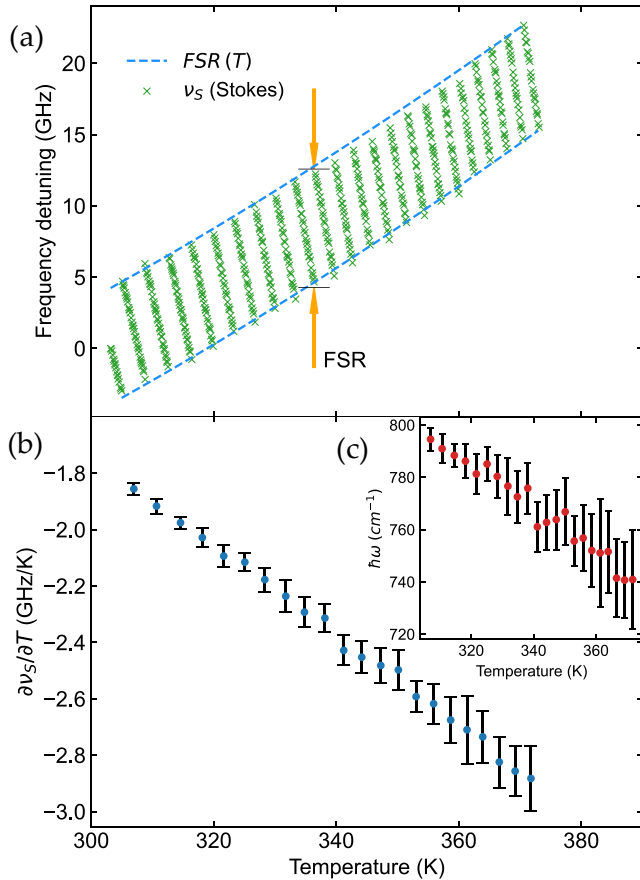


FIG. 4. (a) Stokes center frequency ( $\nu_S$ ) detuning as a function of measured diamond temperature. Dashed blue line represents the tuning range (FSR) of the Stokes frequency as a function of temperature. (b) Measured tuning slope for each FSR as a function of temperature. (c) Calculated average phonon frequencies by solving Eq. (16).

the optical properties of diamond under stimulated Raman scattering conditions. The Raman medium was a synthetic diamond cuboid crystal with dimensions  $7 \times 2 \times 2 \text{ mm}^3$  (FSR at  $573 \text{ nm} \approx 8 \text{ GHz}$ ), plane cut for beam propagation along the 110 axis, and end faces repolished with a parallelism better than  $0.5 \mu\text{m}/\text{mm}$ . The experimental setup can be appreciated in Fig. 2.

Due to the high Raman gain of diamond at  $532 \text{ nm}$ , the Fresnel reflectivity of the uncoated surfaces ( $R_1, R_2 \approx 18\%$ ) was sufficient to ensure highly efficient Raman operation. The diamond crystal was placed on a copper mount inside a high-precision oven (Covesion Ltd), with a temperature standard deviation of less than  $< 10 \text{ mK}$ . Note that the relatively small thermal expansion coefficient of diamond [36,45] and dispersion [46] provided the necessary stability and robustness to perform our measurements accurately.

The pump is a frequency-doubled Nd:YAG  $532 \text{ nm}$  laser generating  $10 \text{ ns}$  pulses at a repetition rate of  $100 \text{ Hz}$  with an energy of  $50 \mu\text{J}$ . The pulses passed through a power control system consisting of a half-wave plate (HWP1) and polarizing beam splitter (PBS). The polarization was controlled by means of another half-wave plate (HPW2); note that the SRS process efficiency depends on polarization and is maximized

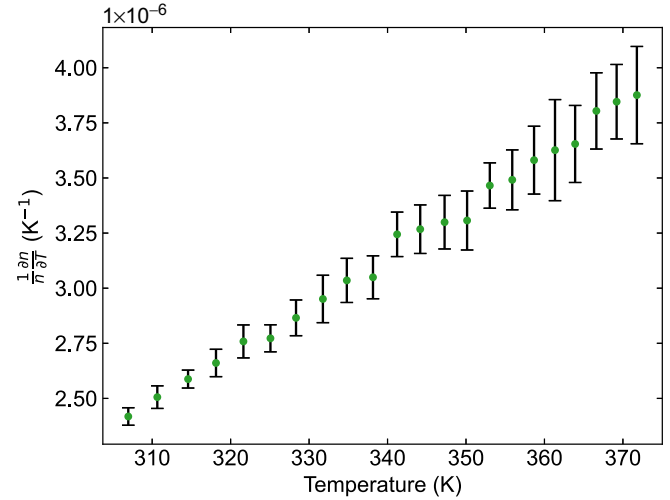


FIG. 5. Calculated thermo-optic coefficient of diamond as a function of temperature between  $300$  and  $370 \text{ K}$  using the solutions of Eq. (16).

when the pump polarization angle is parallel to the 111 crystallographic axis. The pump then arrives at the resonator and goes through the SRS process.

The pump was focused into the diamond crystal by a  $150 \text{ mm}$  focal length lens (FL), producing a waist of  $50 \pm 5 \mu\text{m}$  in diameter and a resulting intensity of  $0.1 \text{ GW}/\text{cm}^2$ . After the generation of the first and second Stokes we used dichroics to filter the undesired Stokes orders. The resulting  $573 \text{ nm}$  beam was then guided to the wavemeter, calibrated power meter (PM), photodiode (PD), and beam profiler. The linewidth (FWHM) of the  $573 \text{ nm}$  Stokes light was measured with a wavelength meter LM-007 wavemeter and was  $100 \pm 20 \text{ MHz}$  averaged over  $\sim 1000$  shots (shown inset in Fig. 3), whereas the center frequency deviation ( $\delta\nu_S$ ) had an root-mean-square value  $< 4 \text{ MHz}$  over more than  $16 \text{ h}$  when actively stabilized using temperature as shown in Fig. 3.

The results of the measurement of the resonating Stokes wavelength with temperature are shown in Fig. 4(a). The tests were carried out by adjusting the temperature setting of the oven in increments of  $10 \text{ mK}$ . The average frequency-temperature tuning slope within a FSR of the resonator was approximately  $\partial\nu_S/\partial T \approx -2.3 \text{ GHz}/\text{K}$ , whereas the temperature dependence of the first-order Raman phonon line was about  $\partial\nu_R/\partial T \approx +0.23 \text{ GHz}/\text{K}$ . This agrees reasonably with calculations resulting from the Klemens model ( $\approx +0.2$  to  $0.25 \text{ GHz}/\text{K}$  between  $300$  and  $400 \text{ K}$ ).

Figure 4(b) shows the measured slope in each FSR as a function of temperature. It can be appreciated that the overall tuning slope increases in absolute value as a function of temperature due to the temperature dependency of the thermo-optic coefficient. The slope in the tuning curves varies significantly from  $-1.8 \text{ GHz}/\text{K}$  to  $-2.8 \text{ GHz}/\text{K}$  in about  $70 \text{ K}$ . The error bars represent the 99% confidence interval. The noticeable correlation between temperature and error can lead to the misconception that error is systemic. In reality the reason is that fewer measurements were taken at higher temperatures due to the nonlinear speed of the temperature scan.

We used the values of the slope to calculate then the average phonon frequency  $\hbar\omega(T)$  of each FSR by solving Eq. (16). Figure 4(c) shows the computed values for the phonon frequency  $\hbar\omega(T)$  for each FSR.

We can now proceed to estimate the thermo-optic coefficient directly by deriving Eq. (19) with the values measured for the temperature-dependent average phonon frequency  $\hbar\omega(T)$ . The result of this is shown in Fig. 5. It is important to note that the apparent similarity between Figs. 4 and 5 is due to the weak temperature dependence of the factors of Eq. (16); however, the relationship between them is not linear. Interestingly, the range where the temperature-dependent index of refraction is nonlinear is most severe for temperatures in the range from 200 to 400 K. Below 200 K,  $(1/n)\partial n/\partial T$  is nearly zero, whereas for values above 400 K it asymptotically tends to a constant value, and from our extrapolations tending to approximately  $8 \times 10^{-6} \text{ K}^{-1}$  at high temperatures above 500 K.

## VI. CONCLUSIONS

In this work we studied the relationship between the resonant Stokes wavelength inside a monolithic diamond Raman resonator and temperature. We found that existing models

for the temperature dependency of diamond's refractive index correspond only approximately to observed experimental processes; however, the accuracy in their predictions is poorer in the 300–400 K range, and hence here we experimentally measured it. Since  $\partial v_S/\partial T$  depends directly on the thermo-optic coefficient, we propose to scan the temperature while measuring the resonant Stokes wavelength to recalculate the thermal dependency of diamond's index of refraction in the visible spectral range.

Regarding the flexibility of the proposed method, the combination of very narrow spectral bandwidth and resulting high spectral density from the resonator, alongside the large transparency range of diamond, makes it very versatile and useful at a large range of wavelengths and temperatures. In fact, the constructed Raman laser is characterized by its modest requirements in terms of resonator quality factors, which readily allow for stable and portable operation usable in scientific applications.

Furthermore, we propose a model for estimating the average lattice phonon frequency of diamond under strong SRS conditions. We expect that the presented method and measured diamond thermo-optical parameters will be useful for research related to the development of temperature-sensitive integrated photonic devices in diamond.

- 
- [1] N. Chauhan, A. Isichenko, K. Liu, J. Wang, Q. Zhao, R. O. Behunin, P. T. Rakich, A. M. Jayich, C. Fertig, C. W. Hoyt, and D. J. Blumenthal, Visible light photonic integrated Brillouin laser, *Nat. Commun.* **12**, 4685 (2021).
  - [2] Y. Hu, M. Yu, D. Zhu, N. Sinclair, A. Shams-Ansari, L. Shao, J. Holzgrafe, E. Puma, M. Zhang, and M. Lončar, On-chip electro-optic frequency shifters and beam splitters, *Nature (London)* **599**, 587 (2021).
  - [3] K. K. Mehta, C. Zhang, M. Malinowski, T.-L. Nguyen, M. Stadler, and J. P. Home, Integrated optical multi-ion quantum logic, *Nature (London)* **586**, 533 (2020).
  - [4] X. Yang, Z. Bai, D. Chen, W. Chen, Y. Feng, and R. P. Mildren, Widely-tunable single-frequency diamond Raman laser, *Opt. Express* **29**, 29449 (2021).
  - [5] S. Sarang, O. Kitzler, O. Lux, Z. Bai, R. J. Williams, D. J. Spence, and R. P. Mildren, Single-longitudinal-mode diamond laser stabilization using polarization-dependent Raman gain, *OSA Continuum* **2**, 1028 (2019).
  - [6] X. Yang, O. Kitzler, D. J. Spence, R. J. Williams, Z. Bai, S. Sarang, L. Zhang, Y. Feng, and R. P. Mildren, Single-frequency 620 nm diamond laser at high power, stabilized via harmonic self-suppression and spatial-hole-burning-free gain, *Opt. Lett.* **44**, 839 (2019).
  - [7] O. Lux, S. Sarang, R. J. Williams, A. McKay, and R. P. Mildren, Single longitudinal mode diamond Raman laser in the eye-safe spectral region for water vapor detection, *Opt. Express* **24**, 27812 (2016).
  - [8] D. T. Echarri, K. Chrysalidis, V. N. Fedosseev, B. A. Marsh, R. P. Mildren, S. M. Olaizola, D. J. Spence, S. G. Wilkins, and E. Granados, Broadly tunable linewidth-invariant Raman Stokes comb for selective resonance photoionization, *Opt. Express* **28**, 8589 (2020).
  - [9] K. Chrysalidis, V. N. Fedosseev, B. A. Marsh, R. P. Mildren, D. J. Spence, K. D. A. Wendt, S. G. Wilkins, and E. Granados, Continuously tunable diamond Raman laser for resonance laser ionization, *Opt. Lett.* **44**, 3924 (2019).
  - [10] E. Granados, C. Granados, R. Ahmed, K. Chrysalidis, V. N. Fedosseev, B. A. Marsh, S. G. Wilkins, R. P. Mildren, and D. J. Spence, Spectral synthesis of multimode lasers to the Fourier limit in integrated Fabry–Pérot diamond resonators, *Optica* **9**, 317 (2022).
  - [11] T. Teraji, Ultrapure homoepitaxial diamond films grown by chemical vapor deposition for quantum device application, in *Diamond for Quantum Applications Part I*, Semiconductors and Semimetals, Vol. 103, edited by C. E. Nebel, I. Aharonovich, N. Mizuochi, and M. Hatano (Elsevier, Cambridge, MA, 2020), pp. 37–55.
  - [12] E. Neu and C. Becher, Diamond-based single-photon sources and their application in quantum key distribution, in *Quantum Information Processing with Diamond*, edited by S. Praver and I. Aharonovich (Woodhead Publishing, 2014), pp. 127–159.
  - [13] M. Markham, A. Edmonds, A. Bennett, P.-O. Colard, W. Hillman, and M. Jaszczkowski, CVD diamond for quantum applications, in *Symposium Latsis 2019 on Diamond Photonics—Physics, Technologies and Applications* (Optical Society of America, 2019), p. 135.
  - [14] D. D. Sukachev, A. Sipahigil, C. T. Nguyen, M. K. Bhaskar, R. E. Evans, F. Jelezko, and M. D. Lukin, Silicon-Vacancy Spin Qubit in Diamond: A Quantum Memory Exceeding 10 ms with Single-Shot State Readout, *Phys. Rev. Lett.* **119**, 223602 (2017).
  - [15] E. Granados, G. Stoikos, D. T. Echarri, K. Chrysalidis, V. N. Fedosseev, C. Granados, V. Leask, B. A. Marsh, and R. P. Mildren, Tunable spectral squeezers based on monolithically

- integrated diamond Raman resonators, *Appl. Phys. Lett.* **120**, 151101 (2022).
- [16] T. Ruf, M. Cardona, C. S. J. Pickles, and R. Sussmann, Temperature dependence of the refractive index of diamond up to 925K, *Phys. Rev. B* **62**, 16578 (2000).
- [17] E. Granados, D. J. Spence, and R. P. Mildren, Deep ultraviolet diamond Raman laser, *Opt. Express* **19**, 10857 (2011).
- [18] R. P. Mildren and A. Sabella, Highly efficient diamond Raman laser, *Opt. Lett.* **34**, 2811 (2009).
- [19] D. J. Spence, E. Granados, and R. P. Mildren, Mode-locked picosecond diamond Raman laser, *Opt. Lett.* **35**, 556 (2010).
- [20] W. Lubeigt, G. M. Bonner, J. E. Hastie, M. D. Dawson, D. Burns, and A. J. Kemp, Continuous-wave diamond Raman laser, *Opt. Lett.* **35**, 2994 (2010).
- [21] A. Sabella, J. A. Piper, and R. P. Mildren, Diamond Raman laser with continuously tunable output from 3.38 to 3.80  $\mu\text{m}$ , *Opt. Lett.* **39**, 4037 (2014).
- [22] I. Friel, S. L. Geoghegan, D. J. Twitchen, and G. A. Scarsbrook, Development of high quality single crystal diamond for novel laser applications, *Proc. SPIE* **7838**, 783819 (2010).
- [23] S. Antipov, A. Sabella, R. J. Williams, O. Kitzler, D. J. Spence, and R. P. Mildren, 1.2 kW quasi-steady-state diamond Raman laser pumped by an  $m^2 = 15$  beam, *Opt. Lett.* **44**, 2506 (2019).
- [24] O. Lux, S. Sarang, O. Kitzler, D. J. Spence, and R. P. Mildren, Intrinsically stable high-power single longitudinal mode laser using spatial hole burning free gain, *Optica* **3**, 876 (2016).
- [25] O. Kitzler, J. Lin, H. M. Pask, R. P. Mildren, S. C. Webster, N. Hempler, G. P. A. Malcolm, and D. J. Spence, Single-longitudinal-mode ring diamond Raman laser, *Opt. Lett.* **42**, 1229 (2017).
- [26] M. Li, O. Kitzler, and D. J. Spence, Investigating single-longitudinal-mode operation of a continuous wave second stokes diamond Raman ring laser, *Opt. Express* **28**, 1738 (2020).
- [27] D. J. Spence, Spectral effects of stimulated Raman scattering in crystals, *Prog. Quantum Electron.* **51**, 1 (2017).
- [28] G. P. Dzhotyan, Y. E. D'yakov, I. G. Zubarev, A. B. Mironov, and S. I. Mikhaïlov, Influence of the spectral width and statistics of a stokes signal on the efficiency of stimulated Raman scattering of nonmonochromatic pump radiation, *Sov. J. Quantum Electron.* **7**, 783 (1977).
- [29] V. G. Sidorovich, Reproduction of the pump spectrum in stimulated Raman scattering, *Sov. J. Quantum Electron.* **8**, 784 (1978).
- [30] W. Trutna, Y. Park, and R. Byer, The dependence of Raman gain on pump laser bandwidth, *IEEE J. Quantum Electron.* **15**, 648 (1979).
- [31] C. Warner and B. Bobbs, Effects of off-resonant Raman interactions on multimode Stokes conversion efficiency and output wave front, *J. Opt. Soc. Am. B* **3**, 1345 (1986).
- [32] L. A. Westling and M. G. Raymer, Intensity correlation measurements in stimulated Raman generation with a multimode laser, *Phys. Rev. A* **36**, 4835 (1987).
- [33] Y. Xiong, S. Murphy, J. L. Carlsten, and K. Repasky, Theory of a far-off resonance mode-locked Raman laser in  $\text{H}_2$  with high finesse cavity enhancement, *J. Opt. Soc. Am. B* **24**, 2055 (2007).
- [34] J. Fontanella, R. L. Johnston, J. H. Colwell, and C. Andeen, Temperature and pressure variation of the refractive index of diamond, *Appl. Opt.* **16**, 2949 (1977).
- [35] P. Y. Yu and M. Cardona, Temperature coefficient of the refractive index of diamond- and zinc-blende-type semiconductors, *Phys. Rev. B* **2**, 3193 (1970).
- [36] P. Jacobson and S. Stoupin, Thermal expansion coefficient of diamond in a wide temperature range, *Diam. Relat. Mater.* **97**, 107469 (2019).
- [37] P. Hervé and L. K. J. Vandamme, General relation between refractive index and energy gap in semiconductors, *Infrared Phys. Tech.* **35**, 609 (1994).
- [38] R. Loudon, The Raman effect in crystals, *Adv. Phys.* **13**, 423 (1964).
- [39] J. González, E. Moya, and J. C. Chervin, Anharmonic effects in light scattering due to optical phonons in  $\text{CuGaS}_2$ , *Phys. Rev. B* **54**, 4707 (1996).
- [40] G. Turri, S. Webster, Y. Chen, B. Wickham, A. Bennett, and M. Bass, Index of refraction from the near-ultraviolet to the near-infrared from a single crystal microwave-assisted CVD diamond, *Opt. Mater. Express* **7**, 855 (2017).
- [41] P. G. Klemens, Anharmonic decay of optical phonons, *Phys. Rev.* **148**, 845 (1966).
- [42] A. Debernardi, S. Baroni, and E. Molinari, Anharmonic Phonon Lifetimes in Semiconductors from Density-Functional Perturbation Theory, *Phys. Rev. Lett.* **75**, 1819 (1995).
- [43] M. S. Liu, L. A. Bursill, S. Prawer, and R. Beserman, Temperature dependence of the first-order Raman phonon line of diamond, *Phys. Rev. B* **61**, 3391 (2000).
- [44] V. Leask, A continuously tunable single longitudinal mode diamond Raman laser, Master's thesis, SUPA Department of Physics, University of Strathclyde, Glasgow, 2019.
- [45] C. Moelle, S. Klose, F. Szcs, H. Fecht, C. Johnston, P. Chalker, and M. Werner, Measurement and calculation of the thermal expansion coefficient of diamond, *Diam. Relat. Mater.* **6**, 839 (1997).
- [46] Diamond Materials, *The CVD Diamond Booklet* (Diamond Materials, Advanced Diamond Technology, Freiburg, 2004), [https://www.diamond-materials.com/site/assets/files/1095/cvd\\_diamond\\_booklet.pdf](https://www.diamond-materials.com/site/assets/files/1095/cvd_diamond_booklet.pdf).